



1 **Temperature seasonality in the North American continental** 2 **interior during the early Eocene climatic optimum**

3 Ethan G. Hyland^{1,2*}, Katharine W. Huntington¹, Nathan D. Sheldon³, Tammo Reichgelt⁴

4 ¹Department of Earth & Space Sciences, University of Washington, Seattle, WA 98195

5 ²Department of Marine, Earth & Atmospheric Sciences, North Carolina State University, Raleigh, NC 27695

6 ³Department of Earth & Environmental Sciences, University of Michigan, Ann Arbor, MI 48104

7 ⁴Lamont Doherty Earth Observatory, Columbia University, Palisades, NY 10964

8 *Correspondence to: Dr. Ethan G. Hyland (ehyland@ncsu.edu)*

9

10 **Abstract.** Paleogene greenhouse climate equability has long been a paradox in paleoclimate
11 research. However, recent developments in proxy and modeling methods have suggested that
12 strong seasonality may be a feature of at least some greenhouse periods. Here we present the first
13 multi-proxy record of seasonal temperatures during the Paleogene from paleofloras, paleosol
14 geochemistry, and carbonate clumped isotope thermometry in the Green River Basin (Wyoming,
15 USA). These combined temperature records allow for the reconstruction of past seasonality in
16 the continental interior, which shows that temperatures were warmer in all seasons during the
17 peak early Eocene climatic optimum and that the mean annual range of temperature was high,
18 similar to the modern value (~26°C). Proxy data and downscaled Eocene regional climate model
19 results suggest amplified seasonality during greenhouse events. Increased seasonality
20 reconstructed for the early Eocene is similar in scope to the higher seasonal range predicted by
21 downscaled climate model ensembles for future high-CO₂ emissions scenarios. Overall, these
22 data and model comparisons have substantial implications for understanding greenhouse climates



23 in general, and may be important for predicting future seasonal climate regimes and their impacts
24 in continental regions.

25

26 **1. Introduction**

27 The Paleogene was the last major greenhouse period in Earth's history and is
28 characterized by extreme warming events and resultant biological shifts (e.g., Greenwood and
29 Wing, 1995; Wilf, 2000; Zachos et al., 2001, 2008; McInerney and Wing, 2011), with prolonged
30 warmth during the early Eocene climatic optimum (EECO) peaking from roughly 52 – 50 Ma
31 (e.g. Zachos et al., 2008; Hyland et al., 2017). The early Eocene in general is thought to represent
32 a warm and “equable” global climate state with high mean annual temperatures (MAT; e.g.,
33 Wilf, 2000; Zachos et al., 2008), low mean annual range of temperatures (MART; e.g., Wolfe,
34 1978, 1995; Greenwood and Wing, 1995), and low pole-to-equator temperature gradients (LTG;
35 e.g., Spicer and Parrish, 1990; Greenwood and Wing, 1995; Evans et al., 2018). While high
36 MAT during the Eocene now seems well established, the feasibility of “equable” conditions
37 defined by low MART and low LTG is still in question as a result of increasingly complex
38 global climate models which are unable to reproduce such conditions (e.g., Barron, 1987; Sloan
39 and Barron, 1990; Sloan, 1994; Huber and Caballero, 2011; Lunt et al., 2012).

40 Recent proxy work on Paleogene warm intervals and hyperthermals such as the
41 Paleocene-Eocene thermal maximum (PETM) has suggested that continental interiors may
42 maintain higher or near-modern MART during these periods, implying that the “low seasonality”
43 aspect of climate equability may not be reasonable under all greenhouse conditions (e.g., Snell et
44 al., 2013; Eldrett et al., 2014). Despite this suggestion, it remains unclear whether proxy
45 estimates from other basins, regions, and greenhouse periods can be reconciled with the range of
46 feasible conditions provided by climate model studies. Quantitative reconstructions of



47 seasonality (MART) based on precise proxy estimates of mean annual temperature (MAT),
48 warm month mean temperature (WMMT), and cold month mean temperature (CMMT) could
49 help to resolve some of these model-proxy discrepancies by providing a robust and well-
50 constrained set of seasonal observations for comparison to available climate model outputs.
51 Robust proxy reconstructions of seasonality are crucial for understanding this aspect of past
52 greenhouse equability (Lunt et al., 2012; Snell et al., 2013; Peppe, 2013).

53 Seasonality estimates have previously been made using a variety of proxy
54 paleothermometers in isolation, and can now be made with higher confidence using recently
55 developed methods that target each of these individual temperature parameters: MAT can be
56 estimated using a paleosol geochemistry-based thermometer, WMMT can be estimated using the
57 carbonate clumped isotope (Δ_{47}) thermometer, and CMMT can be estimated using a nearest
58 living relative (NLR) floral coexistence thermometer. The bulk major-element geochemistry of
59 modern soils has been used to quantify the effects of weathering processes via a wide range of
60 geochemical indices (see Sheldon and Tabor, 2009). The relationship between modern climate
61 parameters like temperature and indices such as salinization (Sheldon et al., 2002), the paleosol
62 weathering index (Gallagher and Sheldon, 2013), and the paleosol-paleoclimate model
63 (Stinchcomb et al., 2016) has led to the development of climofunctions for MAT that have been
64 used to estimate paleo-MAT during the Cenozoic (e.g., Retallack, 2007; Takeuchi et al., 2007;
65 Bader et al., 2015; Stinchcomb et al., 2016). The clumped isotope (Δ_{47}) thermometer is based on
66 the temperature-dependent relative enrichment of multiply substituted isotopologues of CaCO_3
67 ($^{13}\text{C}^{18}\text{O}^{16}\text{O}_2$) within the solid carbonate phase, which is independent of the isotopic composition
68 of the water in which the carbonate precipitated (e.g., Ghosh et al., 2006; Eiler, 2007). For
69 pedogenic carbonates in temperate regions, this growth temperature is linked to mean warm



70 season soil temperatures (e.g., Quade et al., 2013; Hough et al., 2014), and has been used to
71 estimate paleo-WMMT during the Cenozoic (e.g., Snell et al., 2013; Garziona et al., 2014). The
72 nearest living relative (NLR) coexistence method has been developed based on the sensitive and
73 highly conserved collective modern cold temperature tolerances of related floras to calculate cold
74 month temperatures (e.g., Wolfe, 1995; Mosbrugger and Utescher, 1997). Those relationships
75 have been refined and used to estimate quantitative paleo-CMMT during the Cenozoic (e.g.,
76 Greenwood et al., 2005; Thompson et al., 2012; Eldrett et al., 2014; Utescher et al., 2014;
77 Greenwood et al., 2017).

78 Here we employ a multi-proxy approach using paleosol geochemistry, clumped isotope,
79 and floral NLR coexistence thermometry methods from the same localities in order to address
80 seasonality in the past, specifically applying it to the issue of early Eocene greenhouse equability
81 in the North American continental interior. We estimate MAT, WMMT, and CMMT throughout
82 the EECO including both defined peak (~51 Ma) and non-peak conditions (e.g., Hyland et al.,
83 2017), and compare the resultant proxy estimates of temperature seasonality (MART) to the
84 modern climate state of the region, as well as to downscaled climate model predictions of
85 temperature seasonality during the Eocene and for future emissions scenarios.

86

87 **2. Methods**

88 The targeted early Eocene locality is the Green River Basin (GRB) in southwestern
89 Wyoming (USA; Figure 1). The GRB sequence is comprised of a series of terrestrial clastic
90 rocks deposited during the early Eocene and EECO as a result of Laramide synorogenic fluvial
91 and lacustrine sedimentation along the margin of endorheic paleo-lake Gosiute (e.g., Clyde et al.,
92 2001; Smith et al., 2008, 2010, 2015). Contemporaneous multi-proxy records of peak and non-



93 peak conditions during the EECO are from the interfingering Wasatch Formation, primarily
94 fluvial sandstones and paleosols of the Ramsey Ranch and Cathedral Bluffs Members, and Green
95 River Formation, primarily lacustrine shales and carbonates of the Wilkins Peak Member (Figure
96 1). The paleosols and pedogenic carbonates were sampled from the Honeycomb Buttes near
97 South Pass, Wyoming (42.24°N, 108.53°W; Hyland and Sheldon, 2013), while the floral
98 assemblages were sampled from the Latham coal (41.68°N, 107.88°W), Sourdough coal
99 (41.91°N, 108.00°W), Niland Tongue (41.06°N, 108.77°W), and Little Mountain quarry
100 (41.28°N, 109.30°W) outside Rock Springs, Wyoming (Figure 1; Wilf, 1998; 2000).

101

102 **2.1 Temperature proxies**

103

104 **2.1.1 Paleosol geochemistry**

105 The bulk major-element geochemistry of modern soils (specifically B horizons) has been
106 used extensively to develop a number of composition-climate relationships, including those
107 predicted by the paleosol-paleoclimate model (PPM_{1.0}), which relates a broad suite of major
108 element compositions to mean annual temperature (among other factors) at the site of soil
109 formation (Stinchcomb et al., 2016). Stinchcomb et al. (2016) developed this nonlinear spline
110 model using the largest available geochemical dataset from 685 modern soils across North
111 America in order to derive proxy relationships between 11 major and minor oxides and MAT.
112 This new proxy is calibrated over a wider range of climatic conditions, soil types, and parent
113 materials than other available proxies (c.f., Sheldon et al., 2002; Gallagher and Sheldon, 2013),
114 and has been validated via independent comparisons in both modern climosequences
115 (Stinchcomb et al., 2016) and Miocene paleosols (Driese et al., 2016). Following associated



116 procedures, our bulk paleosol samples from selected upper Bt horizons of defined Alfisols
117 (described in detail by Hyland and Sheldon, 2013) were prepared for major-element
118 geochemistry by cleaning and grinding to a homogenous powder. Samples were analyzed using
119 lithium borate fusion preparation and X-ray fluorescence (XRF) measurements at ALS Chemex
120 Laboratory (Vancouver, BC), where analytical uncertainty for analyses was maintained at less
121 than 0.1% for all elements, and replicate analyses had a mean standard deviation of 0.8% (*Table*
122 *A.1*). Resultant major and minor elements data were not corrected for loss-on-ignition (e.g.,
123 Stinchcomb et al., 2016), and were input into the open-access PPM_{1.0} model, which produces
124 “low”, “best” and “high” MAT estimates; we present the “high” estimates as MAT here (see
125 *Section 4.1* for explanation; *Table A.1*).

126

127 **2.1.2 Clumped isotope geochemistry**

128 The clumped isotope (Δ_{47}) thermometer is based on the theoretical temperature
129 dependence of the overabundance of multiply substituted carbonate ion isotopologues (primarily
130 $^{13}\text{C}^{18}\text{O}^{16}\text{O}_2^{-2}$) within the solid carbonate phase, which is independent of the isotopic composition
131 of the waters from which the carbonate precipitated (e.g., Schauble et al., 2006; Ghosh et al.,
132 2006; Eiler, 2007). The enrichment of “clumped” isotopologues relative to the abundance
133 expected for a random distribution of isotopes among isotopologues (Δ_{47}) varies with the growth
134 temperature of the sampled carbonate (e.g., Ghosh et al., 2006; Dennis et al., 2011; Zaarur et al.,
135 2013; Kluge et al., 2015; Kelson et al., 2017). Clumped isotope thermometry of soil carbonates is
136 a useful paleoenvironmental proxy in continental settings (e.g., Eiler, 2011; Quade et al., 2013),
137 and studies of recent pedogenic carbonates indicate that their clumped isotope values record
138 environmental temperature conditions during mineral growth. The timing of pedogenic carbonate



139 growth is controlled by a combination of soil moisture, CO₂, temperature, and other factors over
140 10²–10⁴ years (e.g., Cerling, 1984; Cerling and Quade, 1993; Breecker et al., 2009; Zamanian et
141 al., 2016), and clumped isotope analyses show corresponding variability in recorded
142 temperatures (e.g., Peters et al., 2013; Hough et al., 2014; Burgener et al., 2016; Ringham et al.,
143 2016; Gallagher and Sheldon, 2016). However, for pedogenic carbonates forming in forest soils
144 from mid-latitude regions, this growth temperature has been shown to be linked to mean warm
145 season soil temperatures in most settings (e.g., Breecker et al., 2009; Passey et al., 2010; Quade
146 et al., 2013; Garzione et al., 2014; Hough et al., 2014; Ringham et al., 2016), and has been used
147 to estimate paleo-WMMT during the Cenozoic (e.g., Suarez et al., 2011; Snell et al., 2013;
148 Quade et al., 2013; Garzione et al., 2014).

149 Pedogenic carbonate nodules from selected Bk horizons (paleosol depths ~20–240 cm)
150 were thin-sectioned and analyzed under transmitted light and cathodoluminescence to identify
151 primary micritic carbonate (Figure 2), which was microdrilled/homogenized for clumped isotope
152 (Δ_{47}) analysis. Extremely shallow (<50 cm) or deep (>200 cm) carbonates were analyzed
153 specifically to examine temperature depth profiles in paleosols (Figure 2), while pedogenic
154 carbonates from commonly sampled depths (50–200 cm; e.g., Cerling, 1984; Koch, 1998;
155 Zamanian et al., 2016) were used for calculating and interpreting paleotemperature records.
156 Powdered samples and carbonate standards were analyzed in replicate at the University of
157 Washington's IsoLab, following methods of Burgener et al. (2016) and Kelson et al. (2017),
158 which are modified after Huntington et al. (2009) and Passey et al. (2010). Briefly, CO₂ is
159 produced from 6–8 mg of pure carbonate reacted in a common phosphoric acid bath (~105%
160 H₃PO₄) at 90°C. Evolved CO₂ is then cleaned via passage through a series of automated
161 cryogenic traps and a cooled (-20°C) Poropak Q column using helium carrier gas through a



162 nickel and stainless steel vacuum line, and the purified CO₂ is transferred to Pyrex break seals.
163 Each sample is then analyzed on a Thermo MAT253 mass spectrometer equipped with an
164 automated 10-port tube cracker inlet system and configured to measure m/z 44–49, using data
165 acquisition methods and scripts presented by Schauer et al. (2016).

166 All analyses include an automatically-measured pressure baseline (PBL; He et al., 2012),
167 are corrected using heated gas (1000°C; Huntington et al., 2009) and CO₂-water equilibration
168 (4°C, 60°C) lines during the corresponding analysis period, and are reported in the absolute
169 reference frame (ARF; Dennis et al., 2011). Following recent work (Daëron et al., 2016; Schauer
170 et al., 2016), mass spectrometer data are corrected using the ¹⁷O correction values recommended
171 by Brand et al. (2010). Carbonate standards for these analyses include international standards
172 NBS-19 and ETH-2, as well as internal standards C64 and COR, which are all reported relative
173 to VPDB (δ¹³C, δ¹⁸O) and ARF (Δ₄₇) in *Table B.1*. All samples were analyzed in replicate (3–5)
174 to minimize standard analytical error, and data were reduced following Schauer et al. (2016).
175 Carbonate growth temperatures (T[Δ₄₇]) were calculated using the most current and extensive
176 inorganic calcite calibration (Kelson et al., 2017), which was produced using the updated ¹⁷O
177 correction values of Brand et al. (2010) and is consistent with our analytical methods. Based on
178 preliminary comparisons, the Kelson et al. (2017) calibration produces results not significantly
179 different from data calculated using previous calibrations at moderate Earth-surface temperatures
180 (Daëron et al., 2016; C. John and M. Daëron, pers. comm., 2016; *Table B.1*).

181

182 **2.1.3 Floral coexistence analysis**

183 Floral physiognomy and floral coexistence techniques are often applied in concert to
184 arrive at terrestrial paleoclimate estimates (e.g. Spicer et al., 2014; Reichgelt et al., 2015; West et



185 al., 2015). While floral leaf physiognomy has been used to develop character-climate
186 relationships for parameters like CMMT and MART (e.g., Wolfe, 1995; Wolfe et al., 1998;
187 Wing, 1998), other work has raised questions about the reliability of modern calibrations and
188 possible covariability of seasonal temperatures recorded by floral methods (Jordan, 1997; Peppe
189 et al., 2010). Similar questions have been raised regarding the nearest living relative (NLR)
190 coexistence method (Grimm and Denk, 2012; Grimm and Potts, 2016). However, recent
191 developments have addressed these issues including: 1) improvements or revisions to NLR
192 assignments for paleofloral assemblages (e.g., Manchester et al., 2014; SIMNHP, 2015), 2) new
193 global datasets of modern floral distributions (e.g., TROPICOS, 2015; USDA, 2015, GBIF,
194 2016), 3) high-resolution linked climatic datasets (e.g., Hijmans et al., 2005), and 4) the
195 application of more rigorous statistical analyses (e.g., Eldrett et al., 2014; Utescher et al., 2014;
196 Harbert and Nixon, 2015). As a result of this work, bioclimatic analysis has emerged as a refined
197 version of this approach, employing the climatic range of modern living relatives of plants found
198 together in a fossil assemblage and statistically constraining the most likely climatic co-
199 occurrence envelope (e.g., Greenwood et al., 2005; Thompson et al., 2012; Eldrett et al., 2014;
200 Greenwood et al., 2017).

201 Fossil assemblages were selected from the literature (e.g., Wilf, 1998, 2000) based on
202 temporal fit, floristic diversity, and reliable taxonomy. Fossil taxa were each attributed to a
203 modern taxon based on nearest living relative (e.g., MacGinitie, 1969; Hickey, 1977; Manchester
204 and Dilcher, 1982; Wolfe and Wehr, 1987; Wing, 1998; Wilf, 1998, 2000; Manchester et al.,
205 2014; SIMNHP, 2015), with unattributed or disputed placements assigned conservatively at
206 higher taxonomic levels (*Table C.1*). Climatic envelopes of modern groups in North America
207 and Asia were retained for the ancient taxa based on environmental niche conservation (e.g.,



208 Wang et al., 2010; Fang et al., 2011). Modern taxa distributions (GBIF, 2016) were linked to
209 high-resolution gridded climatic maps (Hijmans et al., 2005) to extract MAT, WMMT and
210 CMMT using the Dismo Package in the R Statistical Program (R Core Team, 2013). Prior to
211 calculating climatic ranges, plant distribution coordinate files were scrutinized for: 1) plants with
212 dubious taxonomic assignments, as not all identifications were rigorous and not all collected
213 specimens were taxonomically assigned by experts (only species-level identifications are
214 included); 2) plants occurring outside of their natural ranges, as many plants occur outside their
215 adapted environment due to agricultural or aesthetic translocation; and 3) redundant occurrences,
216 as many duplicate coordinates or researcher entries exist for the same taxon and their inclusion
217 may skew results toward given localities.

218 Quantitative paleotemperatures were estimated using a modified bioclimatic analysis
219 approach (e.g., Greenwood et al., 2005; Thompson et al., 2012; Eldrett et al., 2014; Greenwood
220 et al., 2017). Overlap ranges of climatic tolerances for coexisting species from each assemblage
221 were defined by calculating probability density functions of those climatic envelopes (Figure 3
222 and *Table C.2*) consistent with recent work (e.g., Thompson et al., 2012; Harbert and Nixon,
223 2015; Grimm and Potts, 2016; Greenwood et al., 2017). In order to avoid inclusion of apparent
224 coexistence intervals in which no modern occurrence is recorded, we calculate the collective
225 probability density of taxa co-occurrence for each combination of MAT (x), WMMT (y), and
226 CMMT (z):

227
$$f(x|t) = \frac{1}{\sqrt{2\sigma^2\pi}} e^{-\frac{(x-\mu)^2}{2\sigma^2}} \quad (1)$$

228
$$f(y|t) = \frac{1}{\sqrt{2\sigma^2\pi}} e^{-\frac{(y-\mu)^2}{2\sigma^2}} \quad (2)$$



229
$$f(z|t) = \frac{1}{\sqrt{2\sigma^2\pi}} e^{-\frac{(z-\mu)^2}{2\sigma^2}} \quad (3)$$

230
$$f(x, y, z, t) = \ln \left[(f(x) \times f(y) \times f(z))_{t_1} \times \dots \times (f(x) \times f(y) \times f(z))_{t_n} \right] \quad (4)$$

231 Calculations are repeated such that the likelihood (f) is calculated for each climatic combination,
232 for each taxon (t), dependent on the number of taxa (n), using the mean and standard deviation of
233 each taxon (*Table C.2*). Climate input parameters were individual occurrence data points
234 (~32,000) derived from GBIF (2016), excluding combinations unlikely to represent the climatic
235 envelope of the taxa in the assemblage by calculating a maximum likelihood probability density
236 function that defines a precise estimate of temperature parameters with a low standard deviation
237 for each selected assemblage (Figure 3).

238

239 **2.2 Modern climate data and model downscaling**

240 The modern temperature dataset was derived from 1981–2010 averaged climate normals
241 from National Oceanic and Atmospheric Administration (NOAA) weather observation stations
242 within the Green River Basin ($n = 18$; NCDC, 2010), defined as the area 40.5–43°N by 107–
243 110.5°W (Figure 1). Future model temperature projection results used a 10-model ensemble
244 from the Coupled Model Intercomparison Project Phase 5 (CMIP5) under standard low (RCP4.5)
245 and high (RCP8.5) emissions scenarios (IPCC, 2014). Results were averaged monthly for the
246 final 10 years of the model run (2090–2099) and calculated over the same study area using
247 standard bias-correction and spatial downscaling (BCSD) methods developed by PCDMI (2014).
248 Eocene model temperature results used data from a modified three-dimensional regional climate
249 model (RegCM3; Sewall and Sloan, 2006; Pal et al., 2007) with established Eocene boundary
250 conditions including low (560 ppm; LoCO) and high (2240 ppm; HiCO) atmospheric $p\text{CO}_2$
251 scenarios (Sewall and Sloan, 2006; Thrasher et al., 2009; 2010). Those results were averaged for



252 the final 20 years of the model run at equilibrium and calculated over the same study area (40.5–
253 43°N by 107–110.5°W) by integrating data across grid cells monthly for each model year within
254 the above defined Green River Basin (e.g., Snell et al., 2013). All modern climate normals and
255 model downscaling results are reported in *Table D.1*.

256

257 **3. Results**

258 PPM_{1.0} statistical model results for MAT from these paleosol samples range from 13.5 to
259 17.6°C ($\mu = 15.2^\circ\text{C}$; $\sigma = 1.3^\circ\text{C}$). Uncertainty for these estimates is reported as the root mean
260 squared error of the model fit regression ($\pm 2.5^\circ\text{C}$). Petrographic observation of carbonate nodules
261 from all depths and selected soils identified dominantly micritic textures with minor components
262 of sub-angular quartz grains and occasional sparry ($>20\mu\text{m}$) calcite veins and cements; however,
263 we were able to identify and micro-sample unaltered fine-grained ($<5\mu\text{m}$) calcite material in each
264 of the examined samples ($n = 14$; Figure 2). Clumped isotope Δ_{47} values for these samples range
265 from 0.582 to 0.631‰ ($\mu = 0.607\text{‰}$; $\sigma = 0.014\text{‰}$), which corresponds to an estimated WMMT
266 range of 18 to 34°C ($\mu = 25^\circ\text{C}$; $\sigma = 4^\circ\text{C}$). Uncertainty for these estimates is reported as
267 propagated error from analytical and equilibrated CO₂ reference frame uncertainty (negligible);
268 replicate standard error ($\mu = 0.008\text{‰}$) or standard error from long-term standards, whichever is
269 larger; and calibration standard error (e.g., Kelson et al., 2017); which have a combined error
270 averaging $\pm 3^\circ\text{C}$. Clumped isotope-based temperature depth profiles in the sampled paleosols
271 show no clear trend with depth, and estimates are mostly within error for a given paleosol
272 (Figure 2). Nearest living relative bioclimatic analysis minimum cold tolerances for these
273 samples range from -28 to 24°C ($\mu = 6^\circ\text{C}$; $\sigma = 7^\circ\text{C}$), and maximum warm tolerances range from
274 10 to 43°C ($\mu = 28^\circ\text{C}$; $\sigma = 5^\circ\text{C}$). Probability density functions define bioclimatic envelopes



275 (Figure 3) corresponding to an estimated CMMT range of 4.2 to 7.6°C ($\mu = 5.9^\circ\text{C}$; $\sigma = 1.2^\circ\text{C}$), an
276 MAT range of 15.2 to 18.2°C ($\mu = 16.5^\circ\text{C}$; $\sigma = 1.1^\circ\text{C}$), and a WMMT range of 27.9 to 28.7°C (μ
277 = 28.3°C; $\sigma = 0.3^\circ\text{C}$) for the collective floral assemblages. Uncertainty for these estimates is
278 reported as 2σ for individual assemblage PDF distributions, which average $\pm 2^\circ\text{C}$. Proxy
279 estimates from all three methods show a trend of increasing temperatures from non-peak
280 conditions into the peak EECO (~51 Ma), after which temperatures decreased back to lower
281 values (Figure 4).

282 Modern climate normals averaged monthly for the GRB range from -8.4 to 18.1°C, with
283 a MAT of 4.4°C (*Table D.1*). Downscaled Eocene climate model results averaged monthly for
284 the GRB range from 4 to 24°C (LoCO) and 6 to 30°C (HiCO), with MATs of 13°C and 16°C,
285 respectively (*Table D.1*). Downscaled future climate model results averaged monthly for the
286 GRB range from -5.0 to 20.4°C (RCP4.5) and -2.9 to 24.7°C (RCP8.5), with MATs of 7.1°C and
287 10.6°C, respectively (*Table D.1*). Monthly temperature trends maintain roughly the same shape
288 for modern observational data, future model estimates, and Eocene model estimates. However,
289 the Eocene modeled cases show substantially higher winter temperatures, and in both modern
290 and Eocene modeled cases the higher emission/ $p\text{CO}_2$ scenario shows an enhanced summer signal
291 relative to the lower emission/ $p\text{CO}_2$ scenario from the same time period (Figure 5).

292

293 **4. Discussion**

294

295 **4.1 Temperature estimates**

296 Temperature estimates from the PPM_{1.0} spline model are based on specifically selected
297 uppermost B horizons of paleosols with comparable parent materials. These horizons were



298 selected based on previous work describing and sampling paleosols from the Cathedral Bluffs
299 Member in the GRB (Figure 1; Hyland and Sheldon, 2013), and based on the characteristics of
300 soils sampled for the paleosol paleoclimate model dataset (Stinchcomb et al., 2016), in order to
301 generate the most robust input data for the PPM_{1.0} spline model. While the PPM_{1.0} model
302 produces multiple possible estimates of paleo-MAT, the estimate shown to be most reliable via
303 concurrent comparisons with other paleotemperature methods (paleobotanical and paleosol
304 proxies) is the “high MAT” value we present here (Michel et al., 2014; Stinchcomb et al., 2016;
305 Driese et al., 2016). We further justify our use of the “high” estimate because the PPM_{1.0} training
306 dataset heavily samples soils from temperate regions (specifically the conterminous USA) which
307 tend to have lower MAT ($\leq 10^{\circ}\text{C}$) and therefore could place excess weight on low values in the
308 model predictive space. This sampling bias likely produces the demonstrated pattern of “best”
309 MAT predictions generally exhibiting positive residuals (Stinchcomb et al., 2016), which means
310 that the PPM_{1.0} model would be more likely to skew temperature estimates from paleosol and
311 other modern samples toward lower-than-observed MAT values. The presented mean annual
312 temperatures appear to coincide with a statistical mean between CMMT and WMMT estimates
313 (Figure 4), and also agree within uncertainty with independent MAT estimates from other types
314 of paleosol geochemistry (salinization index, $\delta^{18}\text{O}$; Hyland and Sheldon, 2013) and broadly with
315 updated physiognometric (*Table C.3*; Wilf, 2000) and coexistence analysis paleobotanical
316 estimates from the GRB (Figure 4).

317 Based on the assessment of physical and isotopic data, our sampled pedogenic carbonate
318 nodules appear to be primary records of Earth surface temperatures at the time of their formation.
319 All sampled nodules preserve micritic carbonate, and transmitted light and cathodoluminescence
320 images show limited recrystallization or void-filling spar and no evidence of pervasive



321 remineralization (Figure 2). Isotopic data also suggest primary and uncontaminated carbonate
322 material; Δ_{48} values remain low ($\ll 1\%$; *Table B.1*), indicating a lack of hydrocarbon or sulfide
323 contamination (e.g., Guo and Eiler, 2007; Huntington et al. 2009). Temperature and $\delta^{18}\text{O}$
324 measurements remain well within the range of reasonable terrestrial values, particularly for
325 continental interior basins with seasonal climates (*Table B.1*; e.g., Quade et al., 2013; Hough et
326 al., 2014). Carbonates forming in temperate regions often exhibit summer/warm-month
327 temperatures due to warm, dry conditions and low soil CO_2 concentrations during those months
328 (e.g., Breecker et al., 2009; Quade et al., 2013). Such conditions are predicted for the GRB
329 during the early Eocene based on regional climate models (Thrasher and Sloan, 2009; 2010), and
330 are evident in paleosol features (Clyde et al., 2001; Hyland and Sheldon, 2013) as well as
331 evaporative $\delta^{18}\text{O}$ of source waters from nearby paleo-lakes Gosiute and Uinta (*Table B.1*; e.g.,
332 Sarg et al., 2013; Frantz et al., 2014). Further warm biasing of soil temperature with respect to air
333 temperature can be imparted by radiant ground heating, but such effects are likely negligible in
334 shaded forest soils (e.g., Quade et al., 2013; Ringham et al., 2016). Clumped isotope data from
335 two soil depth profiles collected in the GRB agree within uncertainty below ~ 50 cm (Figure 2),
336 suggesting that surface heating and depth attenuation of surface temperature variability does not
337 significantly affect the samples used for our MART reconstructions (paleosol depths ~ 50 – 200
338 cm; e.g., Ringham et al., 2016).

339 These results imply that the temperatures measured from our pedogenic carbonates
340 broadly reflect warm month mean soil temperatures (WMMT) as observed in other records (e.g.,
341 Peters et al., 2013; Hough et al., 2014; Burgener et al., 2016). Possible exceptions are two
342 samples at the base of the Honeycomb Buttes section (HB-109 and HB-18; *Table B.1*) which
343 appear to correspond to MAT estimates from the same paleosols ($\text{PPM}_{1,0}$; Figure 4). These



344 lowest temperature estimates from the base of the section may be artificially “cool” as a function
345 of seasonal precipitation regimes spreading carbonate formation across other parts of the year,
346 particularly in soils with deeper Bk horizons like these (e.g., Gallagher and Sheldon, 2016).
347 Because of the likely bias toward MAT in these two samples, we exclude them from calculations
348 of WMMT or MART as indicated in Figure 4; additionally, this effect means that all of our
349 clumped isotope-based estimates of WMMT may be artificially low, suggesting that our
350 calculated MART values could represent a minimum value. However, our resultant clumped
351 isotope-based temperature estimates are mostly in agreement with both regional climate model
352 predictions of summer month air temperatures (e.g., Thrasher and Sloan, 2009; Snell et al., 2013)
353 and paleobotanical coexistence estimates of warm month mean temperatures (Figure 4).

354 Paleobotanical coexistence methods have been shown to reconstruct paleo-temperatures
355 robustly, particularly for warm and cold months in well-sampled and taxonomically rich
356 localities such as these (e.g., Thompson et al., 2012; Grimm and Potts, 2016). However,
357 uncertainties may be larger than accounted for by the described statistical methods applied to
358 these assemblages because: 1) many fossil classifications within the GRB assemblages are not
359 directly comparable to or identifiable as extant species, and coexistence analyses at a generic or
360 familial level may introduce bias by broadening the temperature tolerance ranges of most groups
361 (e.g., Wang et al., 2010); and 2) evolutionary or climatic preferences of Paleogene fossil taxa
362 may not be fully conserved in extant groups, introducing potential sources of error (e.g., Fang et
363 al., 2011). If we double estimated error to account for these unquantifiable uncertainties, the
364 collective coexistence probability density functions from these assemblages still produce
365 CMMT, MAT, and WMMT estimates defined by narrow “maximum likelihood” bioclimatic
366 envelopes ($< \pm 3^{\circ}\text{C}$; Figure 3; *Table C.2*), which suggest that the environmental characteristics of



367 these fossil assemblages are well constrained despite some higher-level NLR assignments.
368 Additionally, sampling bias from well-sampled temperate regions (e.g., North America) in the
369 modern GBIF database may place undue weight on the cool end of plant ranges (e.g.,
370 Greenwood et al., 2017), constraining paleotemperature estimates to lower values or smaller
371 ranges than is appropriate. This suggests that, similar to clumped isotope-based estimates, our
372 plant-based MART values could also represent a minimum value. Despite this, paleobotanical
373 coexistence CMMT estimates agree with regional climate model predictions of winter month
374 temperatures in the GRB (e.g., Thrasher and Sloan, 2009; 2010), MAT estimates agree broadly
375 with multiple paleosol-based proxy estimates (Figure 4; Hyland and Sheldon, 2013) and with
376 updated paleobotanical physiognomy estimates (Figure 4; *Table C.3*; Wilf, 2000), and WMMT
377 estimates agree with regional climate model estimates (e.g., Thrasher and Sloan, 2009; Snell et
378 al., 2013) and broadly with clumped isotope-based estimates (Figure 4). Taken together these
379 proxy results paint a consistent picture of Earth-surface temperatures during the early Eocene,
380 despite uncertainties inherent in each individual method.

381

382 **4.2 Temperature seasonality**

383 Because each of these proxies appears to represent different seasonal temperatures
384 robustly, we combine these estimates to produce a new multiply constrained investigation of
385 paleo-MART. By calculating the differences between CMMT from paleobotanical coexistence
386 analysis, MAT from paleosol geochemistry or paleobotanical analyses, and WMMT from Δ_{47}
387 composition or paleobotanical coexistence analysis, we can directly estimate MART in the past
388 and compare differences in seasonal temperatures independent of calculation method (c.f., Snell
389 et al., 2013). In other words, our approach can define MART as: 1) the difference between



390 WMMT and CMMT; or 2) twice the difference between MAT and either WMMT or CMMT,
391 assuming that MAT falls half way between those estimates by definition (Table 1). Because our
392 approach can calculate MART using both methods and an average of multiple proxies, this
393 allows for a wide range of independent checks on our estimates, providing the most robust
394 available paleo-MART (Table 1). Each method provides consistent answers that are statistically
395 indistinguishable for a given time period (Student's *t*-test p-values = 0.4–0.9), lending
396 confidence to calculations which show that MART ranged from 21–26°C during the early
397 Eocene (Table 1). MART was generally slightly lower than modern (~21–23°C) across this
398 interval, but appears to have increased to near-modern ranges during the peak EECO (~26°C;
399 Figure 4; Table 1). The calculated uncertainty of the difference between these populations
400 (S.E.D) is ~4°C, which makes the non-peak and peak intervals statistically distinct though nearly
401 overlapping.

402 Estimates from the lower end of our reconstructed MART range are still higher than
403 MART estimates from individual paleobotanical proxies (15–18°C; e.g., Greenwood and Wing,
404 1995; Wolfe et al., 1998), but compare favorably to estimates from regional climate models with
405 assumed lacustrine or paludal land cover (20–22°C; Thrasher and Sloan, 2010). However,
406 estimates from the higher end of the reconstructed MART range compare more favorably to
407 modeled MART values with assumed woodland or forested land cover (24–26°C; Thrasher and
408 Sloan, 2010; Snell et al., 2013). The transient nature of paleo-lake Gosiute and the variable
409 evolution of environments within the GRB throughout the early Eocene is well documented in
410 stratigraphic archives, indicating that the basin may have been alternately dominated by the
411 paleo-lake or by forested floodplains during this period (Smith et al., 2008; 2014). In this
412 context, our results suggest that both lower (though still in excess of any previous paleobotanical



413 estimates) and higher MART states may in fact be reasonable for this region at different points
414 during the early Eocene as the GRB evolved. Moreover, proxy and modeling work does not
415 appear to be contradictory, instead having captured different portions of the range of possible
416 MART values indicated for the peak vs. non-peak EECO in this part of the continental interior
417 (Figures 4 and 5). Regardless, these results suggest that MART values lower than $\sim 20^{\circ}\text{C}$ (e.g.,
418 Greenwood and Wing, 1995; Wolfe et al., 1998) may be unreasonable during any part of the
419 EECO, even in the context of variable climate and environmental conditions.

420

421 **4.3 Seasonality implications**

422 Our new proxy data and model comparisons have important implications for continental
423 climates, as they suggest two potential characteristics of seasonality in interior regions during
424 warming events: 1) proxies tend to indicate continental temperatures on the high end of modeled
425 ranges in all seasons, and 2) both proxies and regional models indicate that summer temperatures
426 may increase disproportionately, actually broadening MART, at high atmospheric $p\text{CO}_2$. While
427 proxy and model estimates of paleotemperature generally agree through the early Eocene in the
428 GRB, proxy estimates consistently fall in the top half of all modeled values (Figure 5). Although
429 these model and proxy results are not statistically distinct, they may suggest that realistic
430 environmental responses could have a skewed distribution within the range of model-predicted
431 climate outcomes, an observation which has been made previously for other regions and time
432 periods (e.g., Roe and Baker, 2007; Diffenbaugh and Field, 2013).

433 Winter temperatures were generally high during the Eocene (Figures 4 and 5; e.g.,
434 Greenwood and Wing, 1995), but during the peak EECO summer temperatures appear to have
435 increased disproportionately, broadening the range of MART (Figures 4 and 5). Regional Eocene



436 climate model output for the GRB predicts lower MART ($\sim 20^{\circ}\text{C}$) under low $p\text{CO}_2$ conditions
437 (LoCO scenario), and higher MART ($\sim 24^{\circ}\text{C}$) under high $p\text{CO}_2$ conditions (HiCO scenario;
438 Figure 5; *Table D.1*). Therefore, a theoretical transition from lower (≤ 500 ppm) to higher (≥ 1000
439 ppm) atmospheric $p\text{CO}_2$ during the peak EECO (e.g., Hyland and Sheldon, 2013; Jagniecki et al.,
440 2015) could effectively broaden MART and result in extreme summer temperatures during that
441 period, which would be consistent with both regional model and proxy predictions in the GRB
442 (Figure 5). Regional model-proxy agreement on the plausibility of variable moderate to high
443 MART ($20\text{--}26^{\circ}\text{C}$) in continental interiors fits with global simulations employing a reasonable set
444 of radiative forcings and climate sensitivities, which project similar seasonality ranges during
445 this and other greenhouse events (Huber and Caballero, 2011; Lunt et al., 2012). These
446 temperature seasonality estimates also corroborate recent work on other regions and warm
447 periods (e.g., Snell et al., 2013; Eldrett et al., 2014), and further support the interpretation that
448 continental interiors were less “equable” than previously thought under greenhouse conditions
449 (Snell et al., 2013; Peppe, 2013).

450 Increased seasonality and the disproportionate response of summer temperatures during
451 greenhouse climates also has significant implications for predicting future change in continental
452 interiors. Current projections for the next century using downscaled global climate model
453 ensembles (PCDMI, 2014; *Table D.1*) indicate generally increased temperatures and changing
454 seasonality in North America, and GRB temperatures are projected to increase particularly
455 during winter months (Figure 5). However for high emissions scenarios that may be closer in
456 character to greenhouse conditions like the peak EECO or the PETM (RCP8.5; e.g., IPCC, 2007;
457 Lunt et al., 2012), summer temperatures in the GRB increase more strongly, broadening MART
458 (Figure 5; *Table D.1*). This trend in MART from peak EECO proxy data and high-



459 emission/ $p\text{CO}_2$ model simulations in both the future and Eocene suggests a potential atmospheric
460 $p\text{CO}_2$ threshold for enhanced seasonality, and provides support for models and observations
461 indicating that continental interiors may experience more extreme seasonality in the future under
462 heightened greenhouse conditions (e.g., IPCC, 2007; Diffenbaugh and Field, 2013; Diffenbaugh
463 et al., 2017). The mechanism for producing this increased seasonality remains unclear and
464 requires further study in terms of both proxy applications and model development, although
465 changes in land cover may play a crucial role at least in regional variability (Thrasher and Sloan,
466 2010; Diffenbaugh and Field, 2013).

467

468 **5. Conclusions**

469 Estimates of winter (paleofloral NLR coexistence), mean (paleosol geochemistry), and
470 summer (clumped isotope) temperatures from the early Eocene in the Green River Basin of
471 Wyoming (USA) provide new multi-proxy constraints on seasonality (mean annual range of
472 temperature) in terrestrial settings during greenhouse periods. These records show that MART
473 was variable but near (or above) modern values during the early Eocene climatic optimum,
474 confirming both that seasonality in continental interiors may not remain constant, and that EECO
475 conditions likely do not conform to at least the seasonality aspect of greenhouse “equability”.
476 Comparisons between proxy data and regional/downscaled climate models further imply that
477 temperature seasonality may respond differently at low vs. high atmospheric $p\text{CO}_2$. Overall, this
478 suggests that our understanding of past greenhouse climates in continental interiors may be
479 incomplete when it comes to “equability”, and proposes the potential for extreme seasonality in
480 these regions during past warming events and in the future, which likely has important
481 implications for natural ecosystems and human infrastructure.



482 **Data Availability.** Summarized paleosol, isotope, floral, and modeling data are available in the
483 Supplement, and detailed sample or locality data are available from the authors on request.

484

485 **Author Contributions.** EGH, NDS, and KWH designed the study; EGH and NDS collected the
486 samples and conducted fieldwork; EGH conducted laboratory analyses; EGH, KWH, and TR
487 conducted data analyses and reduction; all authors contributed to the writing of the manuscript.

488

489 **Competing Interests.** The authors declare that they have no conflicts of interest.

490

491 **Acknowledgments.** The authors thank D. Peppe, K. Snell, and XXX for manuscript comments;
492 A. Schauer, L. Burgener, and P. Wilf for assistance with proxy data; PCDMI, WCRP, L. Sloan,
493 and J. Sewall for archived modeling datasets; NSF grants EAR-1252064 and 1156134 (KWH),
494 GSA's Farouk El-Baz grant (EGH), and the Quaternary Research Center and Future of Ice
495 Initiative at the University of Washington for funding and support.

496



497 **References.**

- 498 Bader, N.E., Nicolaysen, K.P., Maldonado, R.L., Murray, K.E., and Mudd, A.C.: Extensive
499 middle Miocene weathering interpreted from a well-preserved paleosol, Cricket Flat, Oregon,
500 USA, *Geoderma*, 239, 195–205, 2015.
- 501 Barron, E.: Eocene equator-to-pole surface ocean temperatures: A significant climate problem?,
502 *Paleoceanography*, 2, 729–739, 1987
- 503 Brand, W.A., Assonov, S.S., and Coplen, T.B.: Correction for the ^{17}O interference in $\delta^{13}\text{C}$
504 measurements when analyzing CO_2 with stable isotope mass spectrometry, *Pure Appl. Chem.*,
505 82, 1719–1733, 2010.
- 506 Breecker, D.O., Sharp, Z.D., and McFadden, L.D.: Seasonal bias in the formation and stable
507 isotopic composition of pedogenic carbonate in modern soils from central New Mexico, USA,
508 *Geol. Soc. Am. Bull.*, 121, 630–640, 2009.
- 509 Burgener, L., Huntington, K., Hoke, G., Schauer, A., Ringham, M., Latorre, C., and Diaz, F.:
510 Variations in soil carbonate formation and seasonal bias over >4km of relief in the western
511 Andes (30°S) revealed by clumped isotope thermometry, *Earth Planet. Sc. Lett.*, 441, 188–199,
512 2016.
- 513 Cerling, T.E.: The stable isotopic composition of modern soil carbonate and its relationship to
514 climate, *Earth Planet. Sci. Lett.*, 71, 229–240, 1984.
- 515 Cerling, T.E., and Quade, J.: Stable carbon and oxygen isotopes in soil carbonates, *Geophys.*
516 *Mono.*, 78, 217–231, 1993.
- 517 Clyde, W.C., Sheldon, N.D., Koch, P.L., Gunnell, G.F., and Bartels, W.S.: Linking the
518 Wasatchian/Bridgerian boundary to the Cenozoic Global Climate Optimum: new
519 magnetostratigraphic and isotopic results from South Pass, Wyoming, *Palaeogeogr. Palaeocl.*,
520 167, 175–199, 2001.
- 521 Daëron, M., Blamart, D., Peral, M., and Affek, H.: Absolute isotopic abundance ratios and the
522 accuracy of Δ_{47} measurements, *Chem. Geol.*, 442, 83–96, 2016.
- 523 Dennis, K.J., Affek, H.P., Passey, B.H., Schrag, D.P., and Eiler, J.M.: Defining and absolute
524 reference frame for clumped isotope studies of CO_2 , *Geochim. Cosmochim. Ac.*, 75, 7117–7131,
525 2011.
- 526 Diffenbaugh, N.S., and Field, C.B.: Changes in ecologically critical terrestrial climate
527 conditions, *Science*, 341, 486–492, 2013.
- 528 Diffenbaugh, N.S., Singh, D., Mankin, J.S., Horton, D.E., Swain, D.L., Touma, D., Charland, A.,
529 Liu, Y., Haugen, M., Tsiang, M., and Rajaratnam, B.: Quantifying the influence of global
530 warming on unprecedented extreme climate events, *P. Natl. Acad. Sci. USA*, 114, 4881–4886,
531 2017.



- 532 Driese, S.G., Peppe, D.J., Beverly, E.J., DiPietro, L.M., Arellano, L.N., and Lehmann, T.:
533 Paleosols and paleoenvironments of the early Miocene deposits near Karunga, Lake Victoria,
534 Kenya, *Palaeogeogr. Palaeoclimatol.*, 443, 167–182, 2016.
- 535 Eiler, J.M.: Clumped-isotope geochemistry – The study of naturally-occurring, multiply-
536 substituted isotopologues, *Earth Planet. Sc. Lett.*, 262, 309–327, 2007.
- 537 Eiler, J.M.: Paleoclimate reconstruction using carbonate clumped isotope thermometry: *Quat.*
538 *Sci. Rev.*, 30, 3575–3588, 2011.
- 539 Eldrett, J.S., Greenwood, D.R., Polling, M., Brinkhuis, H., and Sluijs, A.: A seasonality trigger
540 for carbon injection at the Paleocene-Eocene Thermal Maximum, *Clim. Past*, 10, 759–769, 2014.
- 541 Evans, D., Sahoo, N., Renema, W., Cotton, L.J., Muller, W., Todd, J.A., Saraswati, P.K.,
542 Stassen, P., Ziegler, M., Pearson, P.N., Valdes, P.J., and Affek, H.P.: Eocene greenhouse climate
543 revealed by coupled clumped isotope-Mg/Ca thermometry, *P. Natl. Acad. Sci. USA*, 115, 1174–
544 1179, 2018.
- 545 Fang, J., Wang, Z., and Tang, Z.: Atlas of woody plants in China: Distribution and climate,
546 Springer-Verlag (Beijing, CH), 1909 pp., 2011.
- 547 Frantz, C.M., Petryshyn, V.A., Marenco, P.J., Tripatic, A., Berelson, W.M., and Corsetti, F.A.:
548 Dramatic local environmental change during the Early Eocene Climatic Optimum detected using
549 high-resolution chemical analyses of Green River stromatolites, *Palaeogeogr. Palaeoclimatol.*, 405, 1–
550 15, 2014.
- 551 Gallagher, T.M., and Sheldon, N.D.: A new paleothermometer for forest paleosols and its
552 implications for Cenozoic climate, *Geology*, 41, 647–650, 2013.
- 553 Gallagher, T.M., and Sheldon, N.D.: Combining soil water balance and clumped isotopes to
554 understand the nature and timing of pedogenic carbonate formation, *Chem. Geol.*, 435, 79–91,
555 2016.
- 556 Garzzone, C.A., Auerbach, D.J., Smith, J.J., Rosario, J.J., Passey, B.H., Jordan, T.E., and Eiler,
557 J.M.: Clumped isotope evidence for diachronous surface cooling of the Altiplano and pulsed
558 surface uplift of the Central Andes, *Earth Planet. Sc. Lett.*, 393, 173–181, 2014.
- 559 Ghosh, P., Adkins, J., Affek, H., Balta, B., Guo, W., Schauble, E., Schrag, D., and Eiler, J.: ^{13}C -
560 ^{18}O bonds in carbonate minerals: a new kind of paleothermometer, *Geochim. Cosmochim. Ac.*,
561 70, 1439–1456, 2006.
- 562 Global Biodiversity Information Facility (GBIF): Open Access Biodiversity Data: <http://gbif.org>
563 (last accessed July 2016).
- 564 Greenwood, D.R., and Wing, S.L.: Eocene continental climates and latitudinal temperature
565 gradients, *Geology*, 23, 1044–1048, 1995.
- 566 Greenwood, D.R., Archibald, S.B., Mathewes, R.W., and Moss, P.T.: Fossil biotas from the
567 Okanagan Highlands, southern British Columbia and northeastern Washington State: Climates
568 and ecosystems across an Eocene landscape, *Can. J. Earth Sci.*, 42, 167–185, 2005.



- 569 Greenwood, D.R., Keefe, R.L., Reichgelt, T., and Webb, J.A.: Eocene paleobotanical altimetry
570 of Victoria's Eastern Uplands, *Aus. J. Earth Sci.*, 64, 625–637, 2017.
- 571 Grimm, G.W., and Denk, T.: Reliability and resolution of the coexistence approach- A
572 revalidation using modern day data, *Rev. Palaeobot. Palyno.*, 172, 33–47, 2012.
- 573 Grimm, G.W., and Potts, A.: Fallacies and fantasies: the theoretical underpinnings of the
574 coexistence approach for paleoclimate reconstructions, *Clim. Past*, 12, 611–622, 2016.
- 575 Guo, W., and Eiler, J.M.: Temperatures of aqueous alteration and evidence for methane
576 generation on the parent bodies of the CM chondrites, *Geochim. Cosmochim. Ac.*, 71, 5565–
577 5575, 2007.
- 578 Harbert, R., and Nixon, K.: Climate reconstruction analysis using coexistence likelihood
579 estimation (CRACLE): A method for the estimation of climate using vegetation, *Am. J. Bot.*,
580 102, 1277–1289, 2015.
- 581 He, B., Olack, G., and Colman, A.: Pressure baseline correction and high-precision CO₂ clumped
582 isotope (Δ_{47}) analysis by gas-source isotope ratio mass spectrometry, *J. Mass Spectrom.*, 44,
583 1318–1329, 2012.
- 584 Hickey, L.: Stratigraphy and paleobotany of the Golden Valley Formation (early Tertiary) of
585 western North Dakota, *Geol. Soc. Am. Mem.*, 150, 183 pp., 1977.
- 586 Hijmans, R.J., Cameron, S.E., Parra, J.L., Jones, P.G., and Jarvis, A.: Very high resolution
587 interpolated climate surfaces for global land areas, *Intl. J. Climatol.*, 25, 1965–1978, 2005.
- 588 Hough, B.G., Fan, M., and Passey, B.H.: Calibration of the clumped isotope geothermometer in
589 soil carbonate in Wyoming and Nebraska, USA: Implications for paleoelevation and
590 paleoclimate reconstruction, *Earth Planet. Sc. Lett.*, 391, 110–120, 2014.
- 591 Huber, M., and Caballero, R.: The early Eocene equable climate problem revisited, *Clim. Past*, 7,
592 603–633, 2011.
- 593 Huntington, K.W., Eiler, J.M., Affek, H.P., Guo, W., Bonifacie, M., Yeung, L.Y., Thiagarajan,
594 N., Passey, B., Tripathi, A., Daeron, M., and Came, R.: Methods and limitations of clumped CO₂
595 isotope (Δ_{47}) analysis by gas-source isotope ratio mass spectrometry, *J. Mass Spectrom.*, 44,
596 1318–1329, 2009.
- 597 Hyland, E.G., and Sheldon, N.D.: Coupled CO₂-climate response during the Early Eocene
598 Climatic Optimum, *Palaeogeogr. Palaeoclim.*, 369, 125–135, 2013.
- 599 Hyland, E.G., Sheldon, N.D., and Cotton, J.M.: Constraining the early Eocene climatic optimum:
600 A terrestrial interhemispheric comparison: *Geol. Soc. Am. Bull.*, 129, 244–252, 2017.
- 601 Intergovernmental Panel on Climate Change (IPCC): Fourth Assessment Report: Climate
602 Change (AR4), In Pachuari, R.K., and Reisinger, A. (Eds.), IPCC (Geneva, SWI), 104 pp., 2007.
- 603 Intergovernmental Panel on Climate Change (IPCC): Fifth Assessment Report: Climate Change
604 (AR5), In Pachuari, R.K., and Meyer, L.A. (Eds.), IPCC (Geneva, SWI), 151 pp., 2014.



- 605 Jagniecki, E.A., Lowenstein, T.K., Jenkins, D.M., and Demicco, R.V.: Eocene atmospheric CO₂
606 from the nahcolite proxy, *Geology*, 43, 1075–1078, 2015.
- 607 Jordan, G.J.: Uncertainty in paleoclimatic reconstructions based on leaf physiognomy, *Aus. J.*
608 *Bot.*, 45, 527–547, 1997.
- 609 Kelson, J., Huntington, K.W., Schauer, A., Saenger, C., and Lechler, A.: Toward a universal
610 carbonate clumped isotope calibration: Diverse synthesis and preparatory methods suggest a
611 single temperature relationship, *Geochim. Cosmochim. Ac.*, 197, 104–131, 2017.
- 612 Kluge, T., John, C., Jourdan, A., Davis, S., and Crawshaw, J.: Laboratory calibration of the
613 calcium carbonate clumped isotope thermometer in the 25 - 250°C temperature range, *Geochim.*
614 *Cosmochim. Ac.*, 157, 213–227, 2015.
- 615 Koch, P.L.: Isotopic reconstruction of past continental environments, *Annu. Rev. Earth Plant.*
616 *Sci.*, 26, 573–623, 1998.
- 617 Lunt, D., Jones, T., Heinemann, M., Huber, M., LeGrande, A., Winguth, A., Loptson, C.,
618 Marotzke, J., Roberts, C., Tindall, J., Valdes, P., and Winguth, C.: A model-data comparison for
619 a multi-model ensemble of early Eocene atmosphere-ocean simulations: EoMIP, *Clim. Past*, 8,
620 1717–1736, 2012.
- 621 MacGinitie, H.D.: The Eocene Green River Flora of northwestern Colorado and northeastern
622 Utah, University of California Press (Berkeley, CA), 201 pp., 1969.
- 623 Manchester, S., and Dilcher, D.: Pterocaryoid fruits in the Paleogene of North America and their
624 evolutionary and biogeographic significance, *Am. J. Bot.*, 69, 275–286, 1982.
- 625 Manchester, S.R.: Revisions to Roland Brown’s North American Paleocene flora, *Ac. Mus. Natl.*
626 *Prag.*, 70, 153–210, 2014.
- 627 McInerney, F.A., and Wing, S.L.: The Paleocene-Eocene Thermal Maximum: A perturbation of
628 carbon cycle, climate and biosphere with implications for the future, *Ann. Rev. Earth Planet.*
629 *Sci.*, 39, 489–516, 2011.
- 630 Michel, L.A., Peppe, D.J., Lutz, J.A., Driese, S.G., Dunsworth, H.M., Harcourt-Smith, W.,
631 Horner, W.H., Lehmann, T., Nightingale, S., and McNulty, K.P.: Remnants of an ancient forest
632 provide ecological context for Early Miocene fossil apes, *Nat. Commun.*, 5, 3236, 2014.
- 633 Mosbrugger, V., and Utescher, T.: The coexistence approach- a method for quantitative
634 reconstructions of tertiary terrestrial palaeoclimate data using plant fossils, *Palaeogeogr.*
635 *Palaeocl.*, 134, 61–86, 1997.
- 636 National Climatic Data Center (NCDC): United States Climate Normals, 1981–2010:
637 Climatology of the US, National Oceanic and Atmospheric Administration,
638 <http://www.ncdc.noaa.gov/data#normals> (last accessed April 2015).
- 639 Pal, J.S., et al. (19 others): The ICTP RegCM3 and RegCNET: Regional climate modeling for
640 the developing world, *Bull. Am. Meteorol. Soc.*, 88, 1395–1409, 2007.



- 641 Passey, B.H., Levin, N., Cerling, T.E., Brown, F., and Eiler, J.: High-temperature environments
642 of human evolution in East Africa based on bond ordering in paleosol carbonates, *P. Natl. Acad.*
643 *Sci. USA*, 107, 11245–11249, 2010.
- 644 Peppe, D.J., Royer, D.L., Wilf, P., and Kowalski, E.: Quantification of large uncertainties in
645 fossil leaf paleoaltimetry, *Tectonics*, 29, TC3015, 2010.
- 646 Peppe, D.J.: Hot summers in continental interiors: The case against equability during the early
647 Paleogene, *Geology*, 41, 95–96, 2013.
- 648 Peters, N., Huntington, K.W., and Hoke, G.: Hot or not? Impact of seasonally variable soil
649 carbonate formation on paleotemperature and O-isotope records from clumped isotope
650 thermometry, *Earth Planet. Sc. Lett.*, 361, 208–218, 2013.
- 651 Program for Climate Model Diagnosis and Intercomparison (PCMDI): Bias corrected and
652 downscaled World Climate Research Programme’s Coupled Model Intercomparison Project
653 phase 5 (CMIP5) climate projections, http://gdo-dcp.ucllnl.org/downscaled_cmip_projections/,
654 2014.
- 655 Quade, J., Eiler, J., Daeron, M., and Achyuthan, H.: The clumped isotope geothermometer in soil
656 and paleosol carbonate, *Geochim. Cosmochim. Ac.*, 105, 92–100, 2013.
- 657 R Core Team: R: A language and environment for statistical computing: Foundation for
658 Statistical Computing (Vienna, AT), <https://www.r-project.org>, 2013.
- 659 Reichgelt, T., Kennedy, E.M., Conran, J.G., Mildenhall, D.C., and Lee, D.E.: The early Miocene
660 paleolake Manuherikia: vegetation heterogeneity and warm-temperate to subtropical climate in
661 southern New Zealand, *J. Paleolimnol.*, 53, 349–365, 2015.
- 662 Retallack, G.J.: Cenozoic paleoclimate on land in North America, *J. Geol.*, 115, 271–294, 2007.
- 663 Ringham, M.C., Hoke, G.D., Huntington, K.W., and Aranibar, J.N.: Influence of vegetation type
664 and site-to-site variability on soil carbonate clumped isotope records, Andean piedmont of
665 Central Argentina (32–34 °S), *Earth Planet. Sc. Lett.*, 440, 1–11, 2016.
- 666 Roe, G.H., and Baker, M.B.: Why is climate sensitivity so unpredictable?, *Science*, 318, 629–
667 632, 2007.
- 668 Sarg, J.F., Suriamin, H., Tanavsuu-Milkeviciene, K., and Humphrey, J.D.: Lithofacies, stable
669 isotopic composition, and stratigraphic evolution of microbial and associated carbonates, Green
670 River Formation (Eocene), *Am. Assc. Petr. Geol. Bull.*, 97, 1937–1966, 2013.
- 671 Schauble, E.A., Ghosh, P., and Eiler, J.M.: Preferential formation of ^{13}C - ^{18}O bonds in carbonate
672 materials estimated using first-principle lattice dynamics, *Geochim. Cosmochim. Ac.*, 70, 2510–
673 2529, 2006.
- 674 Schauer, A.J., Kelson, J., Saenger, C., and Huntington, K.W.: Choice of ^{17}O correction affects
675 clumped isotope (Δ_{47}) values of CO_2 measured with mass spectrometry, *R. Comm. Mass*
676 *Spectrom.*, 30, 2607–2616, 2016.



- 677 Sewall, J., and Sloan, L.: Come a little bit closer: A high-resolution climate study of the early
678 Paleogene Laramide foreland, *Geology*, 34, 81–84, 2006.
- 679 Sheldon, N.D., and Tabor, N.J.: Quantitative paleoenvironmental and paleoclimatic
680 reconstruction using paleosols, *Earth Sci. Rev.*, 95, 1–52, 2009.
- 681 Sheldon, N.D., Retallack, G.J., and Tanaka, S.: Geochemical climofunctions from North
682 American soils and application to paleosols across the Eocene-Oligocene boundary in Oregon, *J.*
683 *Geol.*, 110, 687–696, 2002.
- 684 Sloan, L.C.: Equable climates during the early Eocene: Significance of regional paleogeography
685 for North American climate, *Geology*, 22, 881–884, 1994.
- 686 Sloan, L.C., and Barron, E.: “Equable” climates during Earth history, *Geology*, 18, 489–492,
687 1990.
- 688 Smith, M.E., Carroll, A.R., and Singer, B.S.: Synoptic reconstruction of a major ancient lake
689 system: Eocene Green River, western United States, *Geol. Soc. Am. Bull.*, 120, 54–84, 2008.
- 690 Smith, M.E., Chamberlain, K.R., Singer, B.S., and Carroll, A.R.: Eocene clocks agree: coeval
691 $^{40}\text{Ar}/^{39}\text{Ar}$, U-Pb, and astronomical ages from the Green River Formation, *Geology*, 38, 527–530,
692 2010.
- 693 Smith, M.E., Carroll, A.R., Scott, J.J., and Singer, B.S.: Early Eocene carbon isotope excursions
694 and landscape destabilization at eccentricity minima: Green River Formation of Wyoming, *Earth*
695 *Planet. Sc. Lett.*, 403, 393–406, 2014.
- 696 Smith, M.E., Carroll, A.R., and Scott, J.J.: Stratigraphic expression of climate tectonism, and
697 geomorphic forcing in an underfilled lake basin: Wilkins Peak Member of the Green River
698 Formation, In Smith, M.E. and Carroll, A.R. (Eds.), *Stratigraphy and Paleolimnology of the*
699 *Green River Formation*, Springer (Dordrecht, NE), 61–102, 2015.
- 700 Smithsonian Institution Museum of Natural History Paleobiology (SIMNHP): Paleobiology
701 Database, Smithsonian Institution (Washington, DC), <http://www.nmnh.si.edu/>, 2015.
- 702 Snell, K.E., Thrasher, B.L., Eiler, J.M., Koch, P.L., Sloan, L.C., and Tabor, N.J.: Hot summers in
703 the Bighorn Basin during the early Paleogene, *Geology*, 41, 55–58, 2013.
- 704 Suarez, M.B., Passey, B.H., and Kaakinen, A.: Paleosol carbonate multiple isotopologue
705 signature of active East Asian summer monsoons during the late Miocene and Pliocene,
706 *Geology*, 39, 1151–1154, 2011.
- 707 Spicer, R.A., and Parrish, J.T.: Late Cretaceous–early Tertiary paleoclimates of northern high
708 latitude: a quantitative view, *J. Geol. Soc.*, 147, 329–341, 1990.
- 709 Spicer, R.A., Herman, A.B., Liao, W., Spicer, T.E.V., Kodrul, T.M., Yang, J., and Jin, J.: Cool
710 tropics in the Middle Eocene: Evidence from the Changchang Flora, Hainan Island, China,
711 *Palaeogeogr. Palaeocl.*, 412, 1–16, 2014.



- 712 Stinchcomb, G.E., Nordt, L.C., Driese, S.G., Lukens, W.E., Williamson, F.C., and Tubbs, J.D.:
713 A data-driven spline model designed to predict paleoclimate using paleosol geochemistry, *Am. J.*
714 *Sci.*, 316, 746–777, 2016.
- 715 Takeuchi, A., Larson, P.B., and Suzuki, K.: Influence of paleorelief on the Mid-Miocene climate
716 variation in southeastern Washington, northeastern Oregon, and western Idaho, USA,
717 *Palaeogeogr. Palaeocl.*, 254, 462–476, 2007.
- 718 Thompson, R.S., Anderson, K.H., Pelletier, R.T., Strickland, L.E., Bartlein, P.J., and Shafer, S.L.:
719 Quantitative estimation of climatic parameters from vegetation data in North America by the
720 mutual climatic range technique, *Quat. Sci. Rev.*, 51, 18–39, 2012.
- 721 Thrasher, B.L., and Sloan, L.C.: Carbon dioxide and the early Eocene climate of western North
722 America, *Geology*, 37, 807–810, 2009.
- 723 Thrasher, B.L., and Sloan, L.C.: Land cover influences on the regional climate of western North
724 America during the early Eocene, *Global Planet. Change*, 72, 25–31, 2010.
- 725 TROPICOS: Global Plant Database: Missouri Botanical Garden (St. Louis, MO),
726 <http://www.tropicos.org/>, 2015.
- 727 United States Department of Agriculture (USDA): The PLANTS Database: NRCS National
728 Plant Data Team (Greensboro, NC), <http://plants.usda.gov>, 2015.
- 729 Utescher, T., Bruch, A., Erdei, B., Francois, L., Ivanov, D., Jacques, F., Kern, A., Liu, Y.,
730 Mossbrugger, V., and Spicer, R.: The Coexistence Approach- Theoretical background and
731 practical considerations of using plant fossils for climate quantification, *Palaeogeogr. Palaeocl.*,
732 10, 58–73, 2014.
- 733 Wang, Q., Ferguson, D.K., Feng, G., Ablav, A.G., Wang, Y., Yang, J., Li, Y., and Li, C.:
734 Climatic change during the Palaeocene to Eocene based on fossil plants from Fushun China,
735 *Palaeogeogr. Palaeocl.*, 295, 323–331, 2010.
- 736 West, C.K., Greenwood, D.R., and Basinger, J.F.: Was the Arctic Eocene 'rainforest' monsoonal?
737 Estimates of seasonal precipitation from early Eocene megafloras from Ellesmere Island,
738 Nunavut, *Earth Planet. Sc. Lett.*, 427, 18–30, 2015.
- 739 Wilf, P.: Using fossil plants to understand global change: Evidence for Paleocene-Eocene
740 warming in the greater Green River Basin of southwestern Wyoming, University of
741 Pennsylvania (Philadelphia, PA), 384 pp., 1998.
- 742 Wilf, P.: Late Paleocene-early Eocene climate changes in southwestern Wyoming:
743 Paleobotanical analysis, *Geol. Soc. Am. Bull.*, 112, 292–307, 2000.
- 744 Wing, S.L.: Late Paleocene-early Eocene floral and climatic change in the Bighorn Basin,
745 Wyoming, In Aubrey, M., Lucas, S., and Berggren, W. (Eds.), Columbia University Press (New
746 York, NY), 380–400, 1998.
- 747 Wolfe, J.A.: A paleobotanical interpretation of Tertiary climates in the Northern Hemisphere,
748 *Am. J. Sci.*, 66, 691–703, 1978.



- 749 Wolfe, J.A.: Paleoclimatic estimates from Tertiary leaf assemblages: *Ann. Rev. Earth Planet.*
750 *Sci.*, 23, 119–142, 1995.
- 751 Wolfe, J.A., and Wehr, W.: Middle Eocene dicotyledonous plants from Republic, northeastern
752 Washington, *USGS Bull.*, 1597, 67 pp., 1987.
- 753 Wolfe, J.A., Forest, C.E., and Molnar, P.: Paleobotanical evidence of Eocene and Oligocene
754 paleoaltitudes in midlatitude western North America, *Geol. Soc. Am. Bull.*, 110, 664–678, 1998.
- 755 Zaarur, S., Affek, H.P., and Brandon, M.: A revised calibration of the clumped isotope
756 thermometer, *Earth Planet. Sc. Lett.*, 382, 47–57, 2013.
- 757 Zachos, J., Pagani, M., Sloan, L., Thomas, E., and Billups, K.: Trends, rhythms, and aberrations
758 in global climate 65 Ma to Present, *Science*, 292, 686–693, 2001.
- 759 Zachos, J.C., Dickens, G.R., and Zeebe, R.E.: An early Cenozoic perspective on greenhouse
760 warming and carbon-cycle dynamics, *Nature*, 451, 279–283, 2008.
- 761 Zamanian, K., Pustovoytov, K., and Kuzyakov, Y.: Pedogenic carbonates: Forms and formation
762 processes, *Earth Sci. Rev.*, 157, 1–17, 2016.



763 **Figure Captions.**

764 **Figure 1.** Map and stratigraphy of the Green River Basin. A) Map of the region, showing major
765 sedimentary basins and topographic highs. Stars show proxy record sampling sites (paleosols in
766 yellow, paleoflora in red), and dashed box is the sampling region for modern climate stations and
767 the downscaling domain for both models. CF = Cordilleran fold-thrust belt, UU = Uinta uplift,
768 WR = Wind River uplift, OC = Owl Creek uplift, GM = Granite Mountains, FR = Front Range.
769 B) Simplified stratigraphy of the central to eastern GRB, showing facies for the Green River
770 Formation (GRF) and the equivalent and interfingering Wasatch Formation (WF) based on the
771 work of Smith et al. (2015) and Hyland and Sheldon (2013). LY = Lysitean, BF = Blackforkian,
772 LU = Luman Member, NT = Niland Tongue, TM = Tipton Member, WPM = Wilkins Peak
773 Member, LA = Laney Member, RR = Ramsey Ranch Member, CB = Cathedral Bluffs Member.
774

775 **Figure 2.** Paleosol carbonate descriptions. A) Paired transmitted light and cathodoluminescence
776 (CL) images of carbonate nodules showing primary micrite in sampled nodules (I-II) and
777 diagenetically altered material in unsampled nodules (III-IV). Images taken on a Premier ELM-
778 3R Luminoscope at 8–10 kV, 0.5 mA, and 6.6–13.3 Pa with preset 1 s exposure; scale bars ~50
779 μm . B) Clumped isotope-based soil temperature profiles from discrete layers sampled within
780 analyzed paleosol exemplars. Profile HB-129 contained nodular carbonate layers at 20–30 cm,
781 50–65 cm, and 80–100 cm; Profile HB-187 contained nodular carbonate layers at 150–170 cm,
782 190–205 cm, and 240–260 cm.
783

784 **Figure 3.** Floral methods description. A) Probability density functions of hypothetical Taxa A
785 and B along climatic variable X to form a PDF representative of the maximum likelihood of co-



786 occurrence. B) Hypothetical climatic envelope of Taxon Q with climatic variables X and Y,
787 where point R occurs outside the envelope of Taxon Q but within its range of both variables
788 (creating a false inclusion of point R). C) Probability density function distributions for seasonal
789 temperatures from sampled paleofloral sites, where arrows indicate calculated mean
790 temperatures for each parameter.

791

792 **Figure 4.** Temperature proxy estimates of CMMT (white), MAT (gray), and WMMT (black)
793 through the early Eocene. Triangles represent paleobotanical coexistence estimates, squares
794 represent paleosol geochemistry estimates, stars represent revised paleobotanical physiognomy
795 estimates, and circles represent clumped isotope estimates. Error bars represent PDF 2σ
796 (paleobotanical coexistence), root mean squared error (PPM_{1.0} paleosol geochemistry),
797 calibration standard error (paleobotanical physiognomy), and propagated analytical/calibration
798 error (clumped isotopes). Shading highlights peak EECO conditions based on previous work
799 (e.g., Hyland et al., 2017), and dashed line highlights exclusion of two data points (see
800 Discussion). Estimates of peak EECO (51 ± 0.5 Ma) and non-peak EECO MART are defined as
801 described in Table 1 and the Discussion, with MAT shown by vertical lines. Modern MART and
802 MAT are from averaged climate normals for NOAA weather stations in the GRB (NCDC, 2010).
803

804 **Figure 5.** Averaged monthly mean temperatures in the GRB, including: modern instrumental
805 data (filled black circles; NCDC, 2010); high (red squares; RCP8.5) and low (red circles;
806 RCP4.5) future emissions scenarios (PCDMI, 2014); high (blue squares; HiCO) and low (blue
807 circles; LoCO) early Eocene $p\text{CO}_2$ scenarios (Thrasher and Sloan, 2009; 2010); and proxy
808 reconstructions of WMMT and CMMT for non-peak (filled triangles) and peak EECO (open



809 triangles) from this study. Method-averaged MART estimates shown for each category

810 (symbols/colors match main panel).

811

812 **Table 1.** Comparison of Eocene MART estimates using different constraining temperatures and

813 calculation methods.

814

815

816 **Supplement.**

817 **A. Paleosol Data**

818 *Table A.1.* Paleosol geochemistry data

819 **B. Isotope Data**

820 *Table B.1.* Clumped isotope data summary

821 *Table B.2* Clumped isotope data full

822 **C. Floral Data**

823 *Table C.1.* Floral lists and NLR data

824 *Table C.2.* Climatic envelopes for plant taxa

825 *Table C.3.* Mean annual temperature estimates

826 **D. Modeling Data**

827 *Table D.1.* Modern climate data and model outputs



Figure 1.

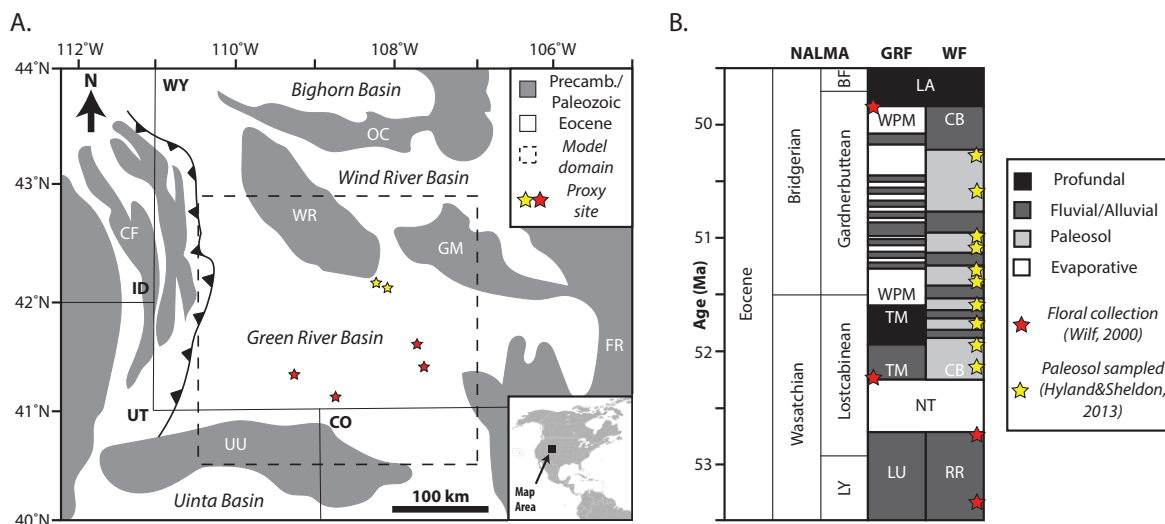




Figure 2.

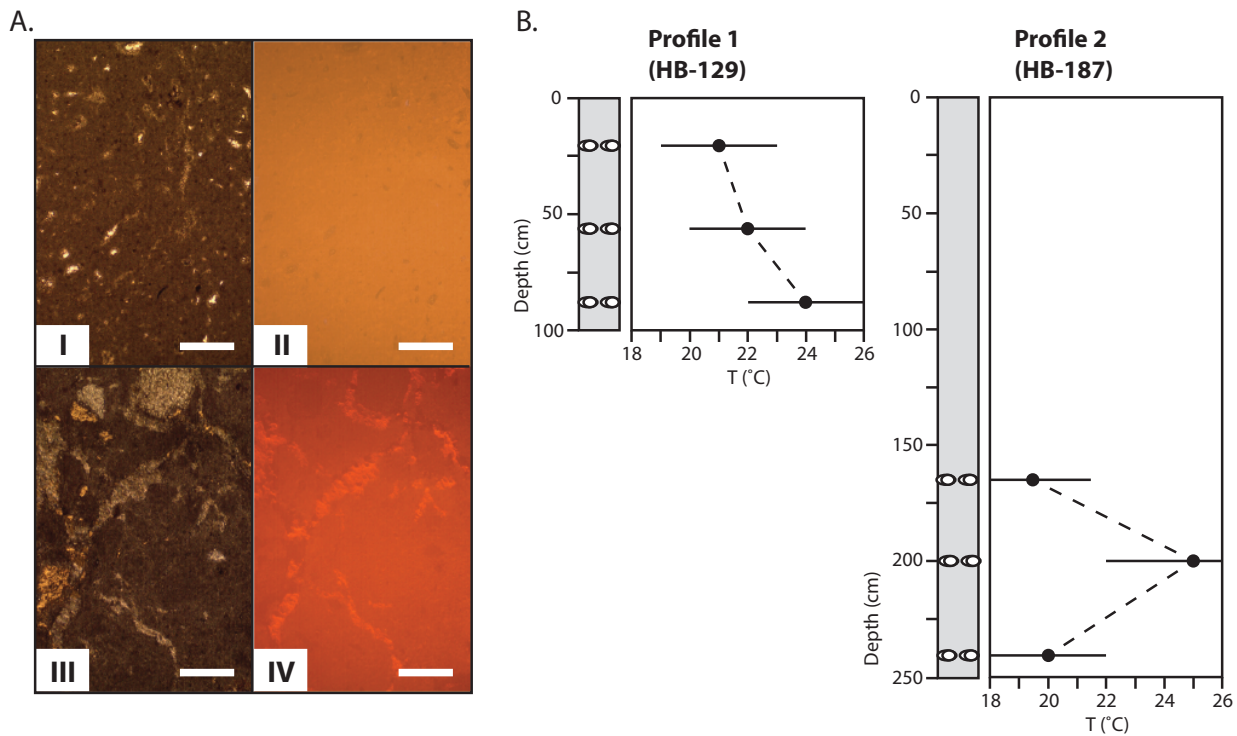




Figure 3.

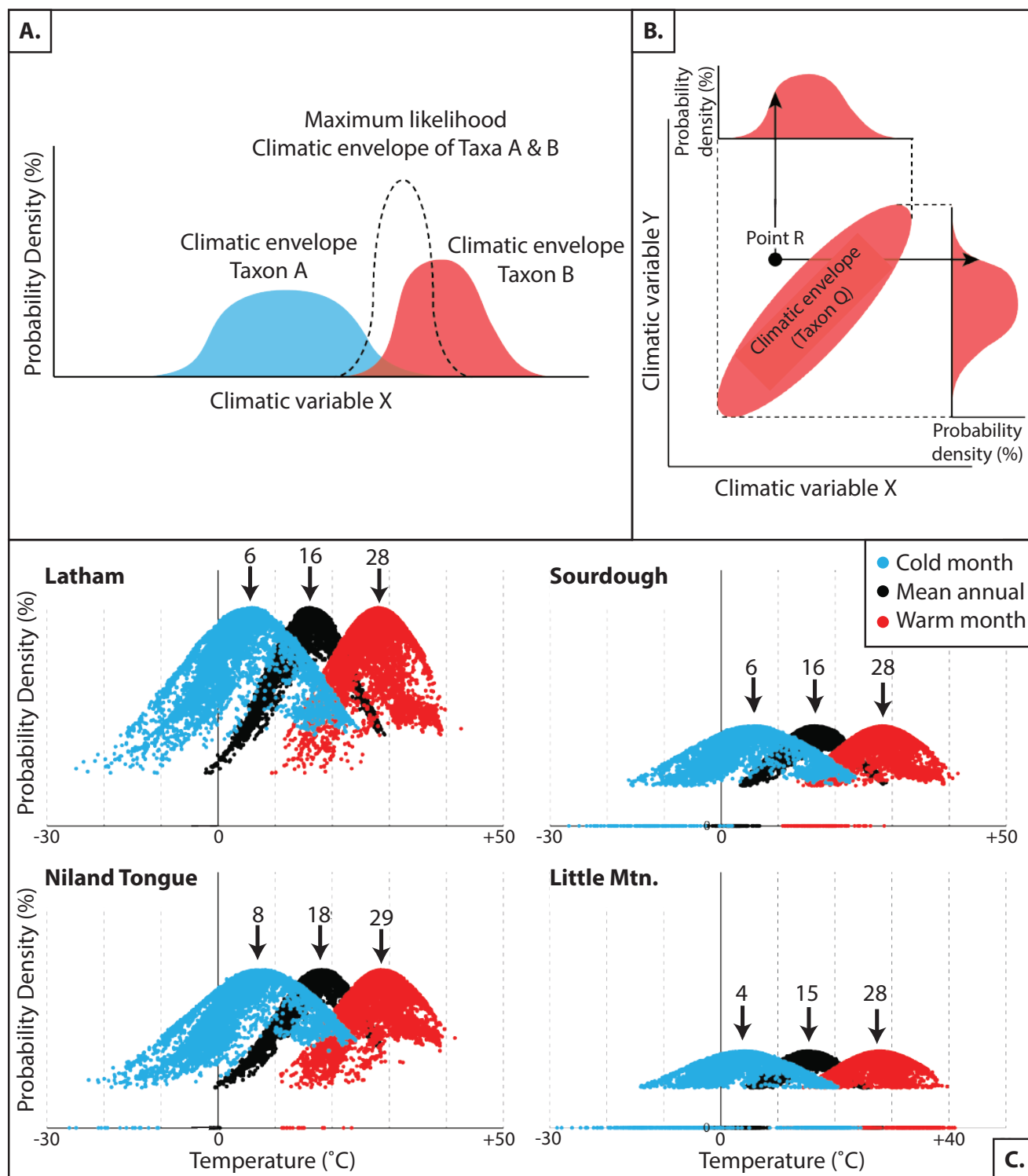




Figure 4.

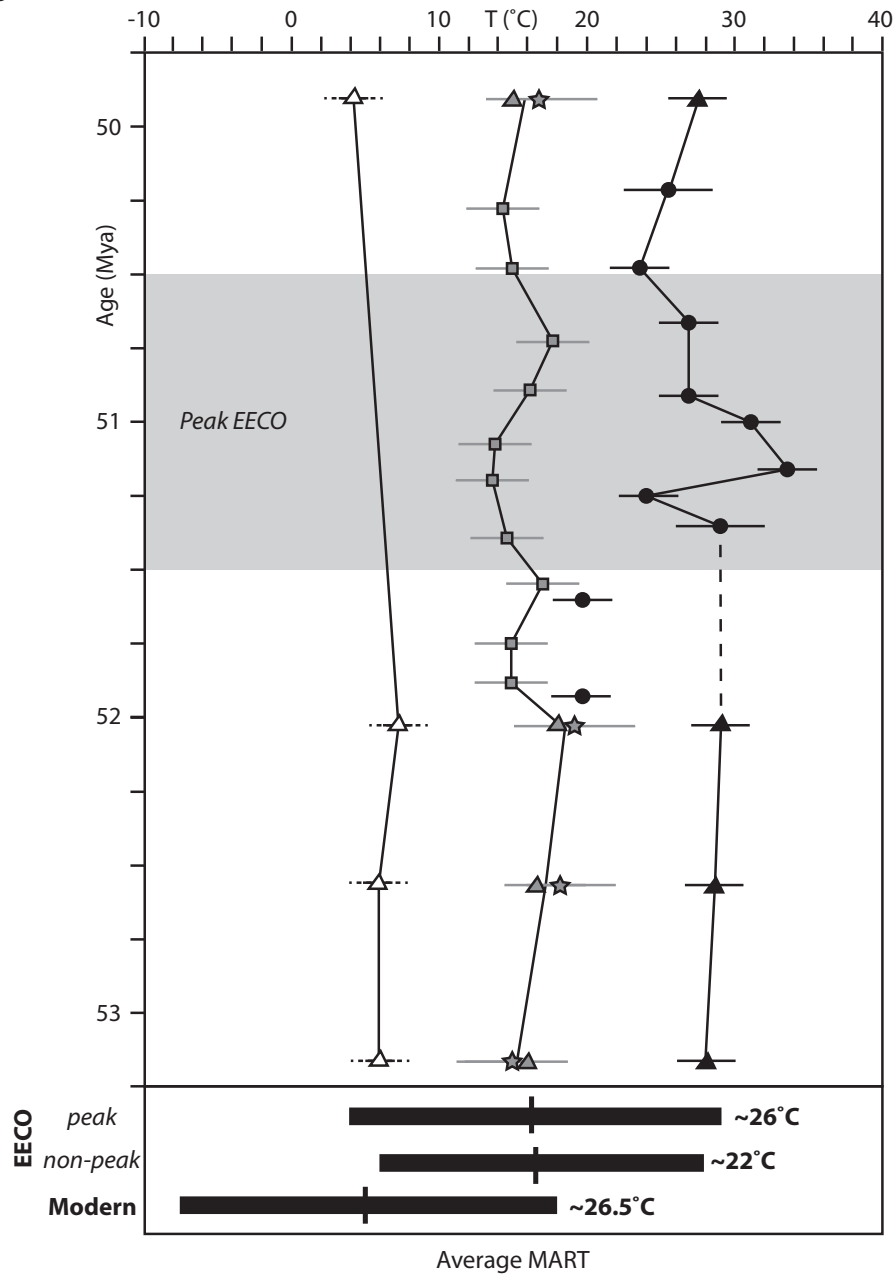




Figure 5.

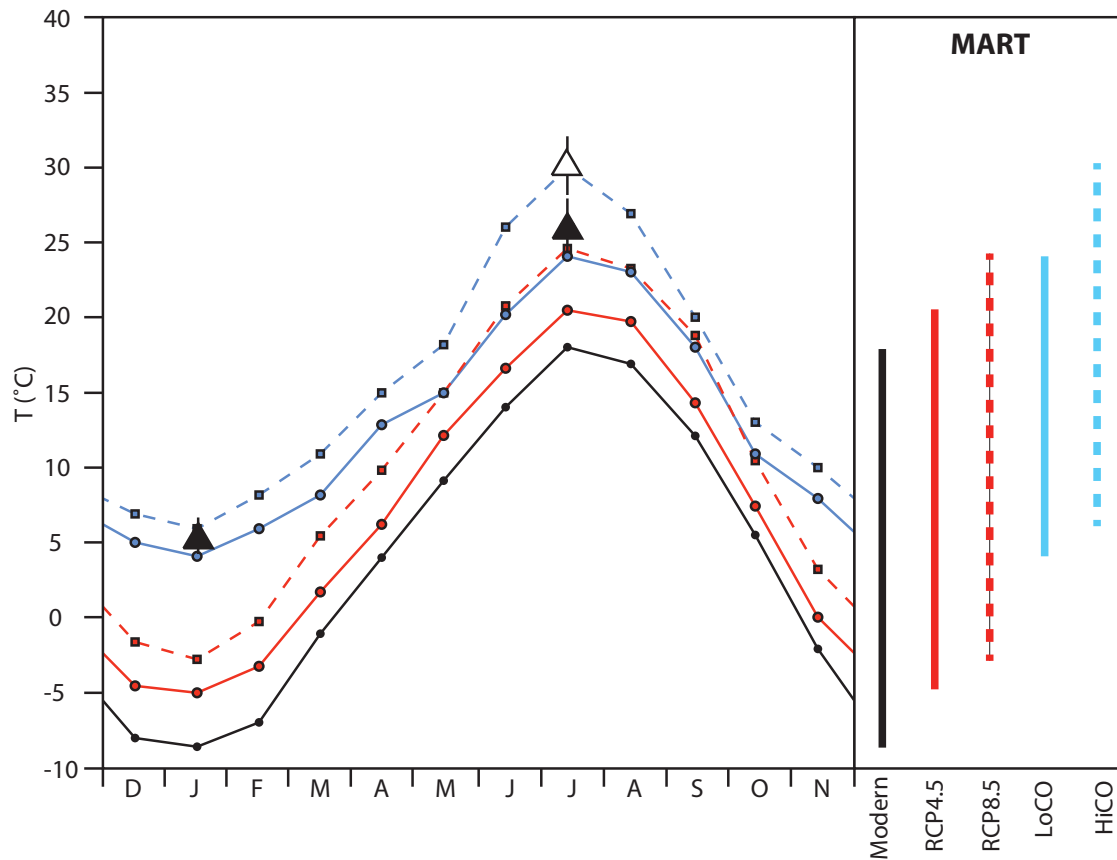




Table 1.

Interval	CMMT*	MAT*	WMMT*	MARTT†	MARTC†	MARTW†
peak EECO (50.5 - 51.5 Ma)	--	15.4°C	28.2°C	--	--	26°C (4)
non-peak EECO (53.5 - 51.5 Ma & 50.5 - 49.5 Ma)	5.9°C	15.6°C	26.8°C	22°C (1)	21°C (1)	23°C (1)

MARTT = WMMT-CMMT

MARTC = (MAT-CMMT)×2

MARTW = (WMMT-MAT)×2

* Average of all available temperature proxy data across indicated time interval.

† Average MART estimate for each calculation method, number in parentheses is S.D. of calculation group.